

Effect of laser irradiation on optical properties of $\text{Ge}_{12}\text{Sb}_{25}\text{Se}_{63}$ amorphous chalcogenide thin films

R Naik^{1*}, S Jena², R Ganesan³ and N K Sahoo²

¹Department of Physics, Utkal University, Bhubaneswar 751004, India

²Atomic and Molecular Physics Division, Bhabha Atomic Research Centre, Mumbai 400085, India

³Department of Physics, Indian Institute of Science, Bengaluru 560012, India

Received: 30 October 2014 / Accepted: 18 February 2015 / Published online: 21 March 2015

Abstract: The change in photo-induced optical properties in thermally evaporated $\text{Ge}_{12}\text{Sb}_{25}\text{Se}_{63}$ chalcogenide thin film under 532-nm laser illumination has been reported in this paper. The structure and composition of the film have been examined by X-ray diffraction and energy dispersive X-ray analysis, respectively. The optical properties such as refractive index, extinction coefficient and thickness of the films have been determined from the transmission spectra based on inverse synthesis method and the optical band gap has been derived from optical absorption spectra using the Tauc plot. It has been found that the mechanism of the optical absorption is due to allowed indirect transition. The optical band gap increases by 0.05 eV causing photo-bleaching mechanism, while refractive index decreases because of reduction in structural disordering. Deconvolution of Raman and X-ray photoelectron spectra into several peaks provides different structural units, which supports the optical photo-bleaching.

Keywords: Chalcogenide; Thin film; Optical properties; Photo-bleaching; Band gap

PACS Nos.: 77.84.Bw; 78.20.-e; 33.20.Ea; 79.60.-i

1. Introduction

Amorphous chalcogenide materials have wide range of technical importance in various solid-state devices. These glassy materials have wide range of transparency in the far infrared region, making them interesting material for various applications. The electrical and the thermal properties of these materials are well studied for their use in application purpose. But, the excellent optical properties make them very useful one. The important features of these semiconducting materials are wide transmission capability (1–20 μm), large refractive index and interesting photo-induced effects [1]. Because of these properties, chalcogenide thin films are interesting candidates for applications in the domain of integrated optics, thermoelectric and solar cell applications [2–4]. Chalcogenide glasses in the system Ge–Sb–Se exhibit attractive optical properties that make them very useful for several applications. The interesting

optical properties such as relatively large band gap, low optical dispersion, low light scattering and long multi-photon edge along with good thermal, mechanical and chemical properties are important for their potential use as optical fibers [5, 6]. The Ge–Sb–Se system is useful due to its robustness, relatively good thermal stability ($T_g \approx 285^\circ\text{C}$ for $\text{Ge}_{28}\text{Sb}_{12}\text{Se}_{60}$), minimized toxicity and broad optical transparency from 700 nm to 16 μm . The basic structural units are Se chains, GeSe tetrahedral and SbSe pyramidal units. The addition of Sb to chalcogenide glass is found to have a variety of applications in optoelectronic devices and optical waveguides. The influence of Ge addition to Sb–Se system and Sb addition to Ge–Se system to form Ge–Sb–Se glass has been studied by various authors [7–9].

The detailed knowledge of the optical properties of these materials is very important in many scientific, technological and industrial applications such as photoconductivity, solar energy, photography, switching, electrophotography, X-ray imaging, photonics, thermal imaging, ultra high density phase change storage and memory, integrated fiber optics,

*Corresponding author, E-mail: ramakanta.naik@gmail.com

infrared photodetectors, photovoltaic and biosensor [10–13]. Among various phenomena happening in the film, photo-induced changes in these chalcogenides are important. The photo-induced effects such as photo-bleaching (PB) and photo-darkening have found potential applications in information storage, photonics, optoelectronics, optomechanical transducers, optical recording, imaging media and absorption filter [14, 15]. The common feature of these glasses is the presence of localized states in the mobility gap, as a result of the absence of long-range order as well as various inherent defects. The presence of lone-pair electrons at the valence band and the structural flexibility associated with the glassy network are mainly responsible for this type of changes. The lone-pair character of the valence tails leads to very rich behavior under the influence of light.

Photo-induced changes in optical transmissivity and reflectivity, index of refraction, changes in reactivity, rates of diffusion and inter-diffusion, viscosity and the state (phase) have been observed in many materials. The optical properties of the Ge–Sb–Se films have been studied for useful applications [16–20]. The study of the optical absorption spectra in chalcogenide glasses provides essential information about the band structure. The optical band gap of the material plays a major role in the preparation of the device for a particular wavelength.

The present paper reports the effect of laser irradiation on the optical properties of amorphous $\text{Ge}_{12}\text{Sb}_{25}\text{Se}_{63}$ thin film. Optical constants such as the refractive index, extinction coefficient or absorption coefficient (α) and thickness of the films have been determined using inverse synthesis method [21] from the transmission spectra measured in the spectral range 600–1100 nm. The optical band gap has been determined from the optical absorption edge using Tauc plot; the Urbach energy has been also calculated from the absorption spectra. Raman and X-ray photoelectron spectra have also studied to support the optical changes.

2. Experimental procedure

Homogeneous $\text{Ge}_{12}\text{Sb}_{25}\text{Se}_{63}$ bulk glasses were prepared by conventional melt quenching method using highly pure (99.999 %) Ge, Se and Sb in appropriate proportions. The mixture was sealed in a quartz glass ampoule under the vacuum of 10^{-5} Torr, which was heated at 950 °C for 36 h in rocking furnace to ensure homogenization of the melt. Quenching was done in ice-cooled water to get the glassy state. $\text{Ge}_{12}\text{Sb}_{25}\text{Se}_{63}$ thin films were prepared by thermal evaporation method at a base pressure of 1×10^{-5} Torr onto the glass substrates (microscope slides) from the prepared bulk glass. The films of uniform thickness were obtained by suitable rotation of the substrate during

Table 1 Measured elemental composition from EDAX for $\text{Ge}_{12}\text{Sb}_{25}\text{Se}_{63}$ thin films

Element	wt%		at%	
	Observed	Calculated	Observed	Calculated
Ge	09.7	10.2	12.1	12
Sb	33.9	34.2	25.1	25
Se	56.4	55.6	62.8	63
Total	100	100	100	100

deposition process. The evaporation rate and thickness (~ 1000 nm) were controlled by using the quartz crystal monitor. The elemental composition of the as-prepared film was checked by energy dispersive X-ray analysis (EDAX) in Sirion XL 40. The scan was done at 20 kV with 40 μA emission current exposing a sample of 1 cm^2 size at 2×10^{-7} Torr pressure. The estimated average precision was <3 % in atomic fraction in each element, as shown in Table 1. The amorphous state of the film was checked by X-ray (Philips type 1710) diffractometer. The films were irradiated at room temperature by a diode-pumped solid-state laser (DPSS) of wavelength 532 nm with a power of 35 mW (5–8 mW near the illuminated spot as measured) to study the photo-induced optical modification in the film. The film was mounted on a sample holder and the laser light was focused on 2-mm-wide spot.

The optical absorption spectra of the as-prepared and illuminated films were taken by using the Fourier transform infrared (FTIR) spectrometer (Bruker Optics (IFS66v/S) in the visible wavelength range of 600–1100 nm at room temperature. XPS measurements were taken to analyze the new bonds formed due to photo-induced effect. It was a useful surface analytical technique to study the chemical state and local environment of an atom. The X-ray photoemission core level spectra were obtained with monochromatic Mg K_{α} X-rays (1253.6 eV) at a vacuum of 10^{-9} Torr in a Multilab 2000 Thermo Scientific UK instrument. The XPS data consisted of survey scans over the entire binding energy (BE) and selected scans over the core level peaks of interest. An energy increment of 1 eV was used for recording the survey spectra and 0.05 eV for the case of core level spectra. The core level peaks were recorded by sweeping the retarding field and using the constant pass energy of 30 eV and the data were averaged over three scans. The reproducibility of the measurements was checked on different regions of the investigated surfaces. For insulators such as glasses, the charging effect could change the BE of the electrons from sample to sample. Hence, the measurement of the absolute BE of electrons from a specified energy level was not reliable. The C 1s line from either adventitious carbon or intentionally added graphite powder on the surface was widely used for charge

referencing [22]. For this study, the adventitious carbon was used as a reference and the BE of the reference C 1s line was set as 284.6 eV. For each sample, a calibration factor was calculated from the difference between the measured C 1s BE and the reference value 284.6 eV [23]. The original BE data were corrected according to the calibration factor. Raman spectroscopic measurements were taken in a Raman spectrometer (LabRAM HR system) using the 514.5-nm argon laser with a CCD detector in backscattering geometry in a range of 50–300 cm^{-1} . The spectral resolution of the spectrometer was 0.5 cm^{-1} . All data were recorded using 2 mW of laser power, which was not sufficient to induce any crystallization in the sample. The intensity of the laser light near the sample was very low and the data acquisition time was within 50 s.

3. Results and discussion

Figure 1 shows X-ray diffraction patterns for as-prepared $\text{Ge}_{12}\text{Sb}_{25}\text{Se}_{63}$ and irradiated thin films. The absence of the diffraction lines in the X-ray pattern indicates amorphous structures of the films. The diffractograms are very similar to the point that no differences can be recorded between the two films. The EDAX analysis carried out on as-prepared and irradiated films suggests that their compositions are very close to the starting materials, as shown in Figs. 2(a) and 2(b). Table 1 confirms the presence of Se, Sb and Ge in the as-deposited films with nearly equal chemical composition.

The optical parameters of the as-prepared and irradiated films are determined from the transmission spectra shown in Fig. 3 using inverse synthesis method [24–27]. The single effective oscillator dispersion model has been considered for determining the optical constants of the as-prepared and irradiated $\text{Ge}_{12}\text{Sb}_{25}\text{Se}_{63}$ thin film. This model

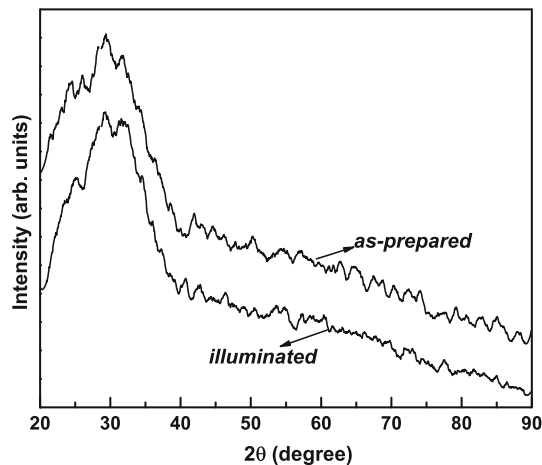


Fig. 1 XRD patterns of the as-prepared and irradiated $\text{Ge}_{12}\text{Sb}_{25}\text{Se}_{63}$ thin films

assumes that the material is composed of individual dipole oscillators that are set to forced vibration by the incident light. Wemple and DiDomenico [28] have proposed that the lowest energy oscillator has the largest contribution to refractive index and the dispersion of refractive index can be described by a single Sellmeier relation given by

$$n^2(\lambda) = 1 + \frac{E_d E_0}{E_0^2 - \left(\frac{hc}{\lambda}\right)^2} \quad (1)$$

The imaginary part of the refractive index, i.e., the extinction coefficient of the films, assumed to follow the Urbach model [29] given by

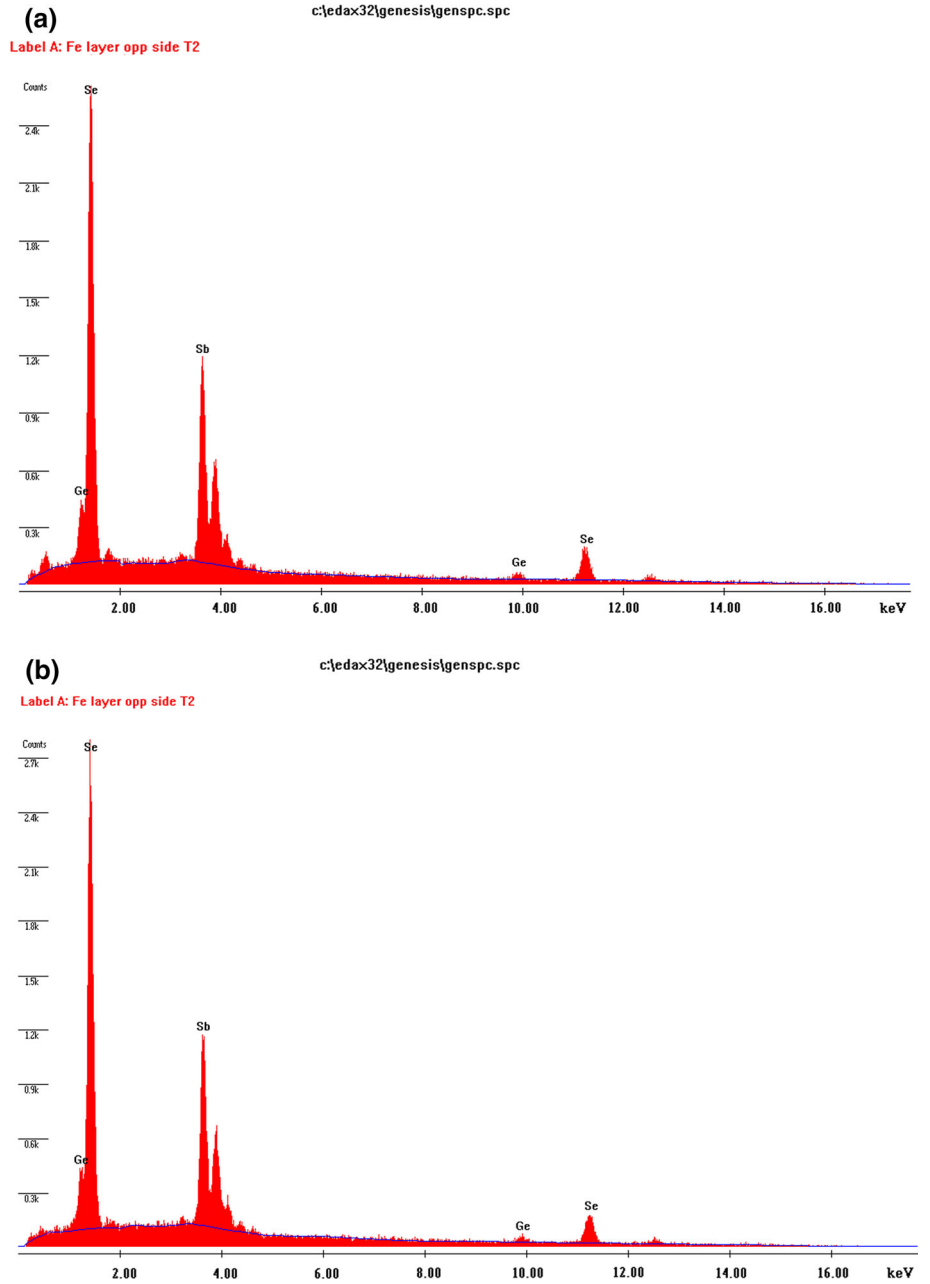
$$k = \alpha \exp\left(12400\beta\left(\frac{1}{\lambda} - \frac{1}{\gamma}\right)\right) \quad (2)$$

where α , β and γ are constants, h is Planck's constant, E_0 is the oscillator energy and E_d is the dispersion energy, which is closely associated with the structural order parameter of the material.

The experimental transmission spectra have been fitted using the coefficient of the dispersion model and the thickness of the film (measured during the deposition of the film) as fitting parameters. Finally, these fitting parameters are used to determine the thickness (t), refractive index (n) and extinction coefficient (k) of the film. The thickness of the as-prepared and irradiated film found from this analysis is given in Table 2. The thickness of the illuminated film decreases after the laser light irradiation [30, 31]. The error in refractive index determined from the transmission spectra using inverse synthesis is negligible and the error of ± 0.01 is only due to the uncertainty in the transmission measurement, i.e., 0.3 %. It is observed that the refractive index of the film decreases with light exposure, which is supported by previous studies on various other types of high intensity photo-exposures as shown in Fig. 4 [32–34]. The decrease in refractive index upon light exposure is due to the decrease in film density, which is a consequence of local structure modification in the film [35]. The photo-induced effect also results in decrease in the film thickness (photo-contraction), as shown in Table 2. The variation in extinction coefficient with wavelength for the as-prepared and irradiated film is shown in Fig. 5. It is clear from this plot that k decreases with wavelength and also decreases upon light exposure, which is a consequence of structural and surface defects caused by light exposure [36].

The dispersion in the material is important for the photonic and telecommunication applications. Wemple–DiDomenico model [28] has been used to determine the dispersion of refractive index [37]. The values of E_0 and E_d are determined from the inverse synthesis method as fitting parameter and are given in Table 2. The static refractive index is calculated from the relation

Fig. 2 EDAX spectrum of the (a) as-prepared $\text{Ge}_{12}\text{Sb}_{25}\text{Se}_{63}$ thin film and (b) irradiated $\text{Ge}_{12}\text{Sb}_{25}\text{Se}_{63}$ thin film



$$n_0^2 = \left(1 + \frac{E_d}{E_0}\right) \quad (3)$$

The values of static refractive index (n_0) and the high frequency dielectric constant $\epsilon_\infty = n_0^2$ for both the as-prepared and irradiated film are given in Table 2. The single oscillator energy E_0 is considered as average energy gap and therefore related to the average molar bond energy of different bonds present in the material. The value of E_0 for as-prepared film decreases with illumination due to the decrease in homopolar bonds such as Sb–Sb, Se–Se and Ge–Ge. It is clear from Table 2 that $E_0 \approx 2^{1.2}E_g$ (approximate), which is in accordance with the findings

reported by others for different materials [33, 37, 38]. The dispersion energy E_d is associated with the change in the structural order of the material and is related to the physical parameters of the material through the following empirical relationship [39]

$$E_d = \beta N_c Z_a N_e \quad (4)$$

where N_c is the effective coordination number of the cation nearest neighbor to the anion, Z_a is the formal chemical valency of the anion, N_e is the effective number of the valance electrons per anion and β is a two-valued constant with either an ionic or covalent value. It is observed that the variation in the dispersion energy E_d results primarily

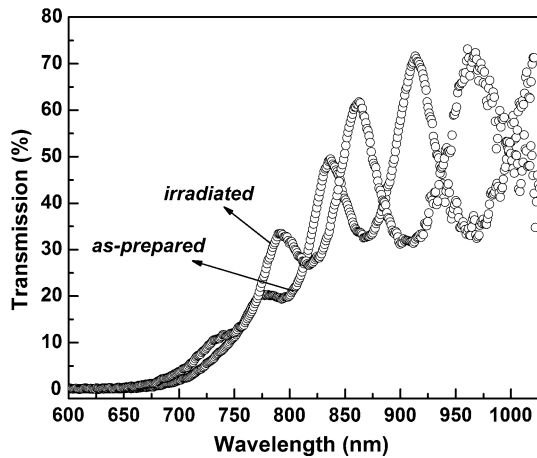


Fig. 3 Experimental transmission spectra of the as-prepared and irradiated $\text{Ge}_{12}\text{Sb}_{25}\text{Se}_{63}$ thin film

from changes in the average nearest neighbor coordination number. So, the increase in dispersion energy E_d is usually associated with evolution of the thin film microstructure to a more ordered phase for which, it is also treated as microstructural order parameter [40]. The E_d for irradiated film is less than that for as-prepared film as shown in Table 2. This indicates that the irradiated film is less structurally ordered than as-prepared film. This local microstructural ordering can predominantly influence the film density, which in turn can lead decrease in refractive index for the irradiated film.

The temperature rise during illumination for the present experimental conditions has been estimated from the formula $\Delta\text{Temp} = I_{\text{abs}}/kr$, where k is the thermal conductivity of the substrate (~ 12.6 mW/cm K for glass), r is the radius of the illuminated light spot (~ 0.20 cm) and I_{abs} is the absorbed light intensity, i.e., $I\alpha d$. Here d , α and I are the film thickness, absorption coefficient and incident power at the spot (~ 8 mW), respectively [41]. Taking the maximum absorption coefficient measured ($\sim 4.1 \times 10^4$ cm^{-1}) in the present work, I_{abs} has been estimated to be 32.8 mW, which gives a temperature rise of ~ 13 K. This small rise in temperature is not large enough to induce any of the observed phenomena reported in this paper. Hence the observed changes are not due to thermal effect but mainly due to photo-induced effects [42].

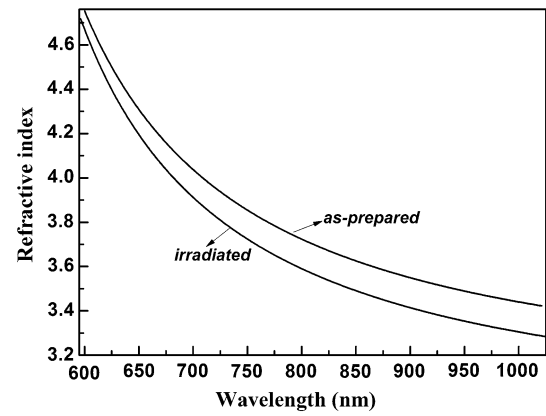


Fig. 4 Variation in n with λ for the $\text{Ge}_{12}\text{Sb}_{25}\text{Se}_{63}$ thin films

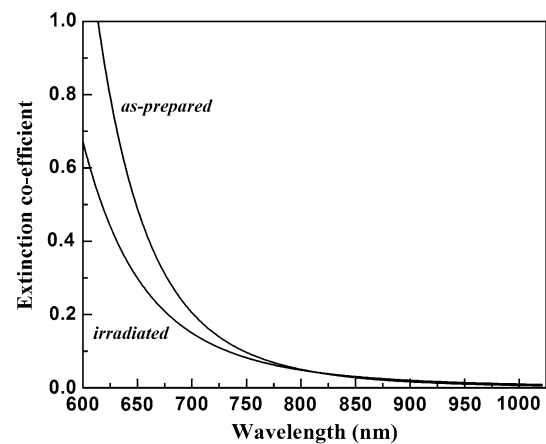


Fig. 5 k versus λ for the $\text{Ge}_{12}\text{Sb}_{25}\text{Se}_{63}$ thin films

The absorption coefficient of amorphous semiconductors in the high absorption region ($\alpha \geq 10^4$ cm^{-1}) follows an exponential law according to Tauc [43],

$$\alpha h\nu = B(h\nu - E_g)^m \quad (5)$$

where B is the constant (Tauc parameter), E_g is the optical energy gap of the material and m determines the type of transition ($m = 1/2$ for direct allowed transition and $m = 2$ for indirect allowed transition) [43, 44]. The best fit of the experimental results of as-prepared and irradiated thin films of $\text{Ge}_{12}\text{Sb}_{25}\text{Se}_{63}$ using Eq. (5), with $m = 2$, i.e., the variation curve of $(\alpha h\nu)^{1/2}$ with photon energy ($h\nu$) shown in Fig. 6 is identical to that of the elemental amorphous

Table 2 Optical parameters of the $\text{Ge}_{12}\text{Sb}_{25}\text{Se}_{63}$ thin films

$\text{Ge}_{12}\text{Sb}_{25}\text{Se}_{63}$ thin film	Film thickness (nm)	Band gap E_g (eV)	Tauc parameter $B^{1/2}$ ($\text{cm}^{-1/2} \text{eV}^{-1/2}$)	Urbach energy (meV)	Dispersion energy E_d (eV)	Oscillator energy E_0 (eV)	Static refractive index (n_0)
As-prepared	1045 ± 3	1.35 ± 0.001	683 ± 3	112 ± 1	28.08 ± 0.001	3.1 ± 0.01	3.17 ± 0.002
Irradiated	1028 ± 4	1.4 ± 0.001	713 ± 2	100 ± 2	28.01 ± 0.002	3.34 ± 0.01	3.06 ± 0.001

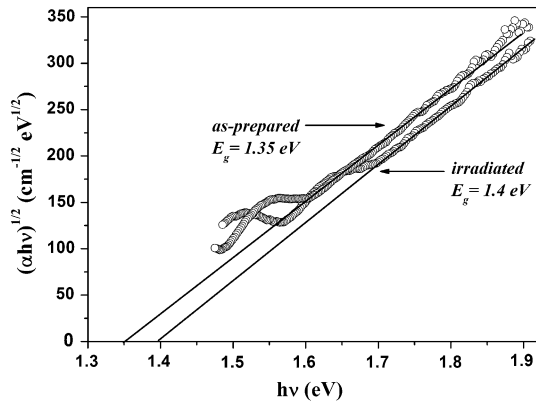
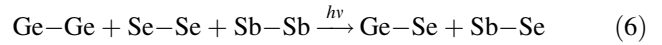


Fig. 6 $(\alpha hv)^{1/2}$ versus (hv) plots for the $\text{Ge}_{12}\text{Sb}_{25}\text{Se}_{63}$ thin films

semiconductor [45]. This indicates that the absorption in as-prepared and irradiated thin films of $\text{Ge}_{12}\text{Sb}_{25}\text{Se}_{63}$ is due to non-direct transition. By plotting $(\alpha hv)^{1/2}$ versus (hv) and fitting the distinct linear regime, which denotes the onset of absorption, with straight line fitting, intercept on X-axis gives the value of optical band gap as shown in Fig. 6. The optical band gaps of the as-prepared and the illuminated films are found to be 1.35 ± 0.001 and 1.4 ± 0.001 eV, respectively, with 0.05 eV increase in the optical band gap, which shows photo-bleaching mechanism in the film. Since the optical absorption depends on the short-range order in the amorphous states and defects associated with it, the increase in optical band gap may be explained on the basis of “density of state model” proposed by Mott and Davis [45]. According to this model, the width of the localized states near the mobility edges depends on the degree of disorder and defects present in the amorphous structure. In particular, it is known that unsaturated bonds together with some saturated bonds are produced as the result of an insufficient number of atoms deposited in the amorphous film [46]. The unsaturated bonds are responsible for the formation of some of the defects in the films, producing localized states in the amorphous materials. The presence of high concentration of localized states in the band structure is responsible for the increase/decrease in optical band gap in the case of the amorphous films. The shift in Fermi level, whose position is determined by the distribution of electrons over the localized states, is also responsible for the increase/decrease in the optical band gap [47]. A decrease in the density of such localized states may enlarge the band gap leading to the blueshift of the electronic absorption edge [48]. The disorder in the as-prepared film is mainly due to the wrong Ge–Ge, Se–Se or Sb–Sb homopolar bonds and Ge(Se) dangling bonds [49]. Therefore, the intrinsic structural change in photo-bleaching process has been proposed as the increase in the Ge–Se, Sb–Se bond density and its subsequent increase in the structural ordering. The intrinsic structural changes are ascribed to the following photoreaction



The illumination process creates local structural ordering in the $\text{Ge}_{12}\text{Sb}_{25}\text{Se}_{63}$ thin films with homopolar bonds Ge–Ge, Se–Se or Sb–Sb being converted into Ge–Se and Sb–Se heteropolar bonds. This observation is in agreement with the fact that the latter bonds are stronger than the former bonds and are more favored as the glass tries to reach the thermal equilibrium of the lowest free energy [31]. The increase in optical band gap (E_g) with laser irradiation (photo-bleaching) can be attributed to the decrease in the density of tail states adjacent to the band edge. The increase in structural ordering due to minimum number of homopolar bonds causes the increase in optical band gap since the state of band tails in the glasses is mainly induced by the homopolar bonds [50]. Generally speaking, an increase in the band gap (blueshift in the absorption edge) is accompanied by decrease in the refractive index according to Moss’s rule ($E_g n^4 \sim \text{constant}$) [51], which we have seen in Fig. 4.

The slope of the Eq. (5) gives the constant $B^{1/2}$, which includes information on the convolution of the valence band and conduction band states and on the matrix element of optical transitions, which reflects not only the k selection rule but also the disorder-induced spatial correlation of optical transitions between the valence band and conduction band [52]. Moreover, B is highly dependent on the character of the bonding. The $B^{1/2}$ for illuminated film ($713 \pm 2 \text{ cm}^{-1/2} \text{ eV}^{-1/2}$) is more than the as-prepared film ($683 \pm 3 \text{ cm}^{-1/2} \text{ eV}^{-1/2}$), which indicates the presence of more number of heteropolar bonds due to chemical orderings in the film. The illuminated film is more ordered (chemically) than the as-prepared film, i.e., the creation of heteropolar bonds after photo-induced process, which is confirmed from the XPS analysis discussed in the present report.

The degree of disorder of the as-prepared and illuminated film also can be analyzed according to the Urbach equation [53]

$$\alpha(h\nu) = \alpha_0 \exp\left(\frac{h\nu}{E_c}\right) \quad (7)$$

where α_0 is a constant and E_c corresponds to the Urbach energy (the width of the band tail of the localized states in the band gap). The above equation describes absorption of the amorphous materials in frequency range $10^0 < \alpha < 10^4 \text{ cm}^{-1}$ [54]. In this region, transition between (defect) states in the gap and the bands takes place. Plotting the dependence of $\log \alpha$ on photon energy gives a straight line. The calculated value of E_c , the inverse of the slope of the straight line, gives the width of the tails of the localized states into the gap at band edges. Urbach energy E_c has been considered as a useful parameter to evaluate the degree of structural disorder

[55]. The value of E_c for as-prepared and illuminated $\text{Ge}_{12}\text{Sb}_{25}\text{Se}_{63}$ film is 112 ± 1 and 100 ± 2 meV, respectively. The lower values of Urbach energy E_c of the illuminated film over the as-prepared film clearly indicate that the illuminated film is more structurally ordered than the as-prepared film, which may be due to the creation of heteropolar bonds after photo-induced process.

As mentioned earlier, XPS spectroscopic technique is used to analyze the new bonds formed between the components due to photo-induced effect. It is a useful surface analytical technique to study the chemical state and local environment of an atom [56]. The chemical bonding is often realized through correlation with chemical shifts in XPS binding energies of the corresponding elements. When the X-ray photon impinges on a sample, photoionization takes place and an electron is expelled from the sample with a certain kinetic energy. The energy of the photoelectrons leaving the sample, gives a spectrum with a series of peaks. The binding energies of the peaks are characteristic of each element. Since XPS is a surface analytical technique, most of spectra come from the top 70–100 Å layer. All the elements have many photoelectron and Auger peaks, but we have considered Ge 3d, Se 3d and Sb 4d core peaks only. For detailed analysis, the spectra have been deconvoluted into its sub-peaks by the XPS data analysis software developed by Kwok called as XPSPEAK. The Shirley baseline has been used for background removal and the deconvoluted peaks have been assumed to have Voigt line shapes. The parameters have been chosen by using pure elemental data as reference and fitting optimization. As the parameters are chosen, the spectra have been then fitted to as few peaks as possible.

The Sb 4d and Ge 3d spectra of the as-prepared and illuminated films are shown in Fig. 7(a). The Se 3d peak position for as-prepared and illuminated films is at 54.72 and 54.10 eV, respectively, as shown in Fig. 7(b). This peak shifting of 0.62 eV toward lower binding energy (BE) shows the formation of Se–Sb and Ge–Se heteropolar bonds due to illumination. Due to spin orbit splitting, Se 3d consists of doublets corresponding to $\text{Se } 3d_{5/2}$ and $\text{Se } 3d_{3/2}$ (intensity ratio 5:3) with a separation of 0.8 eV, which we have observed from the deconvoluted peaks (1, 2 and 1', 2') of the as-prepared samples as shown in Fig. 8(a) and (3, 4 and 3', 4') of the irradiated film as shown in Fig. 8(b). Here, 1 and 2 denote $\text{Se } 3d_{5/2}$ states and 1' and 2' denote $\text{Se } 3d_{3/2}$ for the as-prepared film. Similarly, 3 and 4 denote $\text{Se } 3d_{5/2}$ states and 3' and 4' denote $\text{Se } 3d_{3/2}$ for the irradiated film. The positions of sub-peaks are mentioned in the Figs. 8(a) and 8(b). The two doublets of $\text{Se } 3d_{3/2}$ peak for the irradiated film (54.01 and 55.11 eV) are shifted toward lower BE by ~ 0.61 eV from the as-prepared (54.62 and 55.73 eV) one. Similarly, the shift between the doublets of as-prepared (53.83 and 54.93 eV) and irradiated (53.21 and

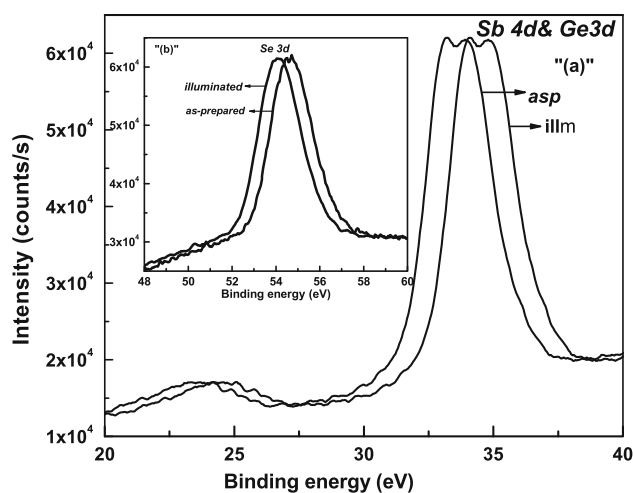


Fig. 7 XPS core level spectra of (a) Ge 3d, Sb 4d and (b) Se 3d of $\text{Ge}_{12}\text{Sb}_{25}\text{Se}_{63}$ thin films

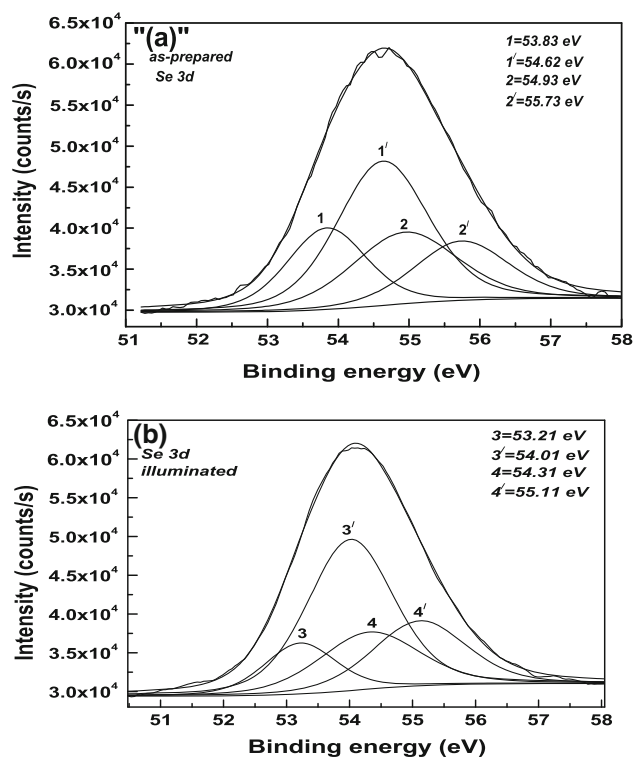


Fig. 8 Deconvoluted XPS spectra of Se 3d (a) as-prepared and (b) illuminated $\text{Ge}_{12}\text{Sb}_{25}\text{Se}_{63}$ thin films

54.31 eV) $\text{Se } 3d_{5/2}$ peak is ~ 0.62 eV. This trend of shifting of BE toward lower energy levels is due to the photo-induced changes in the film, which caused the formation of more number of Sb–Se and Ge–Se bonds rather than the homopolar bonds as suggested by Eq. (6). The shifting in BE of Se 3d peak position toward lower BE due to thermal induced effect in Ge–As–Se system has also been reported [19, 57]. This excess heteropolar bonds in

the irradiated film can change the local microstructure as well as grain morphology, which leads to decrease in film packing density, thus decreasing refractive index. The Sb–Se–Ge film structure can be attributed as being made up of completely cross-linked structure of Sb_2Se_3 and GeSe_3 . The electronegativity of Se (2.55) is much more than that of Sb (2.05) and Ge (2.01) [58]. So, the shifting toward lower BE shows the formation of more number of Ge–Se and Sb–Se heteropolar bonds.

From the Sb 4d and Ge 3d core level XPS spectra for the as-prepared and irradiated film as shown in Fig. 7(a), it is noted that the BE is shifting toward higher energy side for the irradiated sample. The Ge 3d peaks are located around 30–35 eV with a separation of ~ 0.6 eV between Ge $3d_{3/2}$ and Ge $3d_{5/2}$. Sb 4d peaks are located around 30–35 eV with a separation of 1.2 eV between Sb $4d_{3/2}$ and Sb $4d_{5/2}$. As both the core level peaks are situated close to each other, we have deconvoluted the peaks to distinguish from each other as shown in Figs. 9(a) and 9(b). The Sb $4d_{3/2}$ and Sb $4d_{5/2}$ are corresponding to regular Sb atoms within $\text{SbSe}_{3/2}$ pyramids and Ge $3d_{3/2}$ and Ge $3d_{5/2}$ are corresponding to regular Ge atoms within $\text{GeSe}_{4/2}$ tetrahedral. From the spectra of Ge 3d peak, it is found that due to irradiation, the peak is shifting toward the higher BE due to the formation of Ge–Se heteropolar bonds because of the higher binding energy of $\text{GeSe}_{4/2}$ and $\text{SbSe}_{3/2}$ than Ge–Ge- and Sb–Sb-related structure [50]. The Ge 3d peak position for as-prepared and illuminated films is at 33.22 and 33.91 eV, respectively, as shown in Fig. 7(a). The Ge $3d_{3/2}$ and Ge $3d_{5/2}$ peaks for the as-prepared film are at 33.12 and 32.55 eV, respectively. After the irradiation process, these two peaks are shifted to 33.43 and 33.99 eV with a shift of around ~ 0.87 eV. There is also shift in the position of Sb 4d peaks due to illumination process. The peak positions of Sb 4d core level spectra in Fig. 7(a) for as-prepared and illuminated films are at 33.90 and 34.85 eV, respectively. The deconvoluted peaks of Sb 4d core levels of as-prepared and illuminated films are shown in Figs. 9(a) and 9(b). The Sb $4d_{5/2}$ and Sb $4d_{3/2}$ peaks are situated at BE of 33.92 and 35.12 eV with a gap of 1.20 eV. The BE of both the peaks is increased to 34.85 and 36.05 eV, respectively, due to photo-induced process. This peak shifting toward the higher BE is due to the formation of more Sb–Se heteropolar bonds as the electronegativity of Sb is much less than that of Se (2.55). We can also see the peak corresponding to Ge–Se is at 32.55 and 32.98 eV in the as-prepared and irradiated film as shown in Figs. 9(a) and 9(b). The intensity of this peak is more in case of irradiated film, suggesting more number of Ge–Se bonds. Thus, the formation of more number of heteropolar bonds, reduces the disorderness inside the band gap region and increases the optical band gap.

The microstructural changes in $\text{Ge}_{12}\text{Sb}_{25}\text{Se}_{63}$ thin films caused by illumination have been obtained from Raman

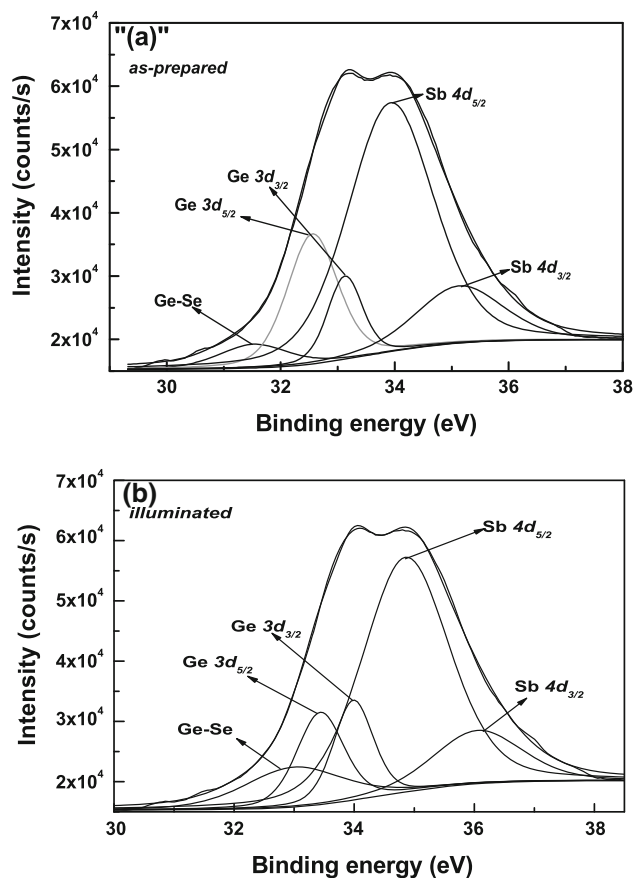


Fig. 9 Deconvoluted XPS spectra of Ge 3d and Sb 4d (a) as-prepared and (b) illuminated $\text{Ge}_{12}\text{Sb}_{25}\text{Se}_{63}$ thin films

spectra as shown in Fig. 10(a). It is well known that for Se-rich Ge–Sb–Se system, the structural model involved is tetrahedral GeSe_2 , pyramidal $\text{SbSe}_{3/2}$ units and cross-linked by Se chain fragments. A dominant band featured around $170\text{--}200\text{ cm}^{-1}$ is formed evidently by overlapping other bands, which can be seen in the deconvoluted spectra as shown in Fig. 10(b). The main band at 186 cm^{-1} can be assigned to Sb–Se bonds' vibration in $\text{SbSe}_{3/2}$ pyramids [16, 59]. The band shifts toward lower wave number and the intensity are increased upon light illumination. This is due to the formation of more Sb–Se heteropolar bonds on the expense of homopolar bonds at 152 cm^{-1} . The band at 152 cm^{-1} is due to vibrational modes of $\text{Se}_2\text{Sb–SbSe}_2$ [58]. The prominent peak for the as-prepared one here is minimized due to the formation of Sb–Se bonds. The band at 172 cm^{-1} is attributed to the stretching vibration of homopolar Ge–Ge and Sb–Sb bonds in the $\text{Ge}_2(\text{Se}_{1/2})_6$ structural units [60]. The vibrational bands at 118 and 205 cm^{-1} are also connected to the presence of Sb–Se stretching modes of $\text{SbSe}_{3/2}$ pyramidal units [60]. The Ge–Se heteropolar bond breathing vibration of edge-sharing $\text{Ge}_2\text{Se}_2\text{Se}_{4/2}$ bitetrahedral is represented by 215 cm^{-1} [61]. The band at 252 cm^{-1} that we have identified with the

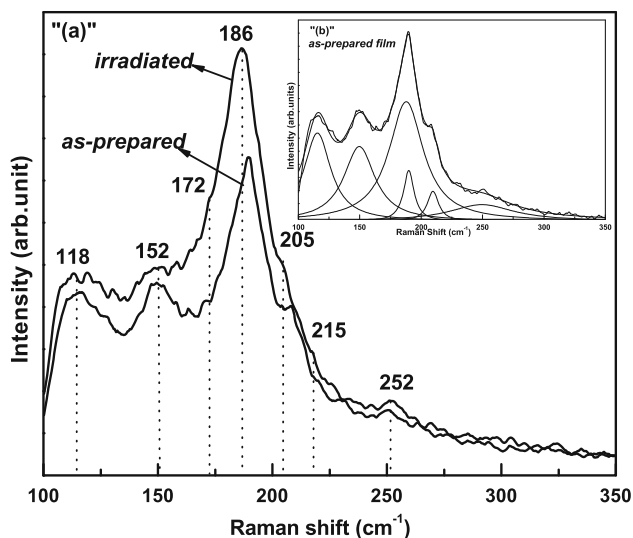


Fig. 10 Raman spectra of (a) as-prepared and illuminated $\text{Ge}_{12}\text{Sb}_{25}\text{Se}_{63}$ thin films and (b) deconvoluted spectra of as-prepared $\text{Ge}_{12}\text{Sb}_{25}\text{Se}_{63}$ thin film

reported band at 250 cm^{-1} is arising from the stretching vibration of Se–Se bonds [62, 63]. We have observed from the vibrational peaks that the Sb–Se bond formation is rather more than that of Ge–Se. The analysis of Raman spectra of both the film suggests that the film structure is modified through a conversion of a pair of homopolar bonds to heteropolar bonds reducing the structural disorder. It should be noted that the minority Ge–Sb heteropolar bonds may not be clearly identified in the present sample.

4. Conclusions

In conclusion, we have observed the photo-induced optical bleaching in thermally evaporated amorphous $\text{Ge}_{12}\text{Sb}_{25}\text{Se}_{63}$ thin films, when exposed to illumination with 532-nm laser. This process has changed the optical transmissivity, optical band gap, $B^{1/2}$, refractive index, extinction coefficient, oscillator energy, dispersion energy, etc. of the films. The illuminated film shows lower refractive index and higher optical band gap than the as-prepared film due to the microstructural as well as chemical ordering in the film. The result is verified by the XPS analysis and is attributed to the creation of heteropolar bonds. The indirect allowed transition occurs in the film. The change in localized states near to the band edges causes the photo-bleaching phenomena. The formation of more heteropolar bonds is realized through the shift in binding energy of core level spectra, which supports the increase in optical band gap. The analysis of Raman spectra of both the film suggests that the film structure is modified through a conversion of a pair of homopolar bonds to heteropolar bonds reducing the structural disorder by laser

illumination. The optical changes in the film can be used effectively for nonlinear optical devices. These types of materials can be used for creation of optical, integrated optical elements, which need high local changes in optical parameters.

Acknowledgments The authors thank Department of Science and Technology (DST), Govt of India, for DST-INSPIRE Research grant and the National Facility for Optical Spectrometry at Department of Physics and Surface Science facility, Indian Institute of Science (IISc), for XPS measurement.

References

- [1] A Uren, A Piarristeguy, M Fontanaa, C Vigreux-Bercovicic, A Pradel and B Arcondo *J. Phys. Chem. Solids* **68** 993 (2007)
- [2] E S M Farag *Opt. Laser Technol.* **36** 35 (2004)
- [3] S K Chakarvarti *Indian J. Phys.* **83** 737 (2009)
- [4] F S Terra, G M Mahmoud, L Mourad and A Tawfik *Indian J. Phys.* **86** 1093 (2012)
- [5] D Rock *Photon. Spectra (USA)* **19** 77 (1985)
- [6] S E Hodges and J Capenter *Proc. SPIE Int. Soc. Opt. Eng. (USA)* **32** 618 (1986)
- [7] W H Wei, L Fang, X Shen and R P Wang *J. Appl. Phys.* **115** 113510 (2014)
- [8] N Sharma, S Sharda, V Sharma and P Sharma *J. Non-Cryst. Solids* **371–372** 1 (2013)
- [9] N Sharma, S Sharda, V Sharma and P Sharma *Mater. Chem. Phys.* **136** 967 (2012)
- [10] R Tintu, V P N Nampoori, P Radhakrishnan and Thomas Sheenu *J. Non-Cryst. Solids* **357** 2888 (2011)
- [11] R Golovchak, O Shpotyuk, M Vlcek, A Ganjoo and H Jain *Philos. Mag.* **87** 4323 (2007)
- [12] B J Eggleton, B Luther-Davies and K Richardson *Nat. Photonics* **5** 141 (2011)
- [13] A B Seddon *J. Non-Cryst. Solids* **184** 44 (1995)
- [14] K Shimakawa, A Kolobov and S R Elliott *Adv. Phys.* **44** 475 (1995)
- [15] P Krecmer, A M Moulin, R J Stephenson, T Rayment, M E Welland and S R Elliot *Science* **277** 1799 (1997)
- [16] Y Chen et al. *J. Alloys Compd.* **548** 155 (2013)
- [17] E S M Farag *Opt. Laser Technol.* **38** 14 (2006)
- [18] W Zhang et al. *Mater. Lett.* **98** 42 (2013)
- [19] R P Wang, D Y Choi, A V Rode, S J Madden and B Luther-Davies *J. Appl. Phys.* **101** 113517 (2007)
- [20] W-H Wei, R-P Wang, X Shen, L Fang and B Luther-Davies *J. Phys. Chem. C* **117** 16571 (2013)
- [21] I Chambouleyron, J M Marinez, A C Moretti and M Mulato *Appl. Opt.* **36** 8238 (1997)
- [22] J F Moulder, W F Sticker, P E Sobol and K D Bomben *Hand Book of X-ray Photoelectron Spectroscopy* (Eden Prairie: Perkin Elmer) (1992)
- [23] T L Barr and S Seal *J. Vac. Sci. Technol. A* **13** 1239 (1995)
- [24] N M Kamble, R B Tokas, A Biswas, S Thakur, D Bhattacharya and N K Sahoo *Vacuum* **86** 422 (2011)
- [25] I Chambouleyron, J M Marinez, A C Moretti and M Mulato *Thin Solid Films* **317** 133 (1998)
- [26] J Maria, G Leal, R P Alcon, J A Angel, D A Minkov and E Marquez *Appl. Opt.* **41** 7300 (2002)
- [27] S Jena, R B Tokas, N Kamble, S Thakur, D. Bhattacharyya and N K Sahoo *Thin Solid Films* **537** 163 (2013)
- [28] S H Wemple and M DiDomenico *Phys. Rev. B* **3** 1338 (1971)

- [29] Y Kuzukawa, A Ganjoo and K Shimakawa *J. Non-Cryst. Solids* **227** 715 (1998)
- [30] R Naik, R Ganesan, K V Adarsh, K S Sangunni, V Takats and S Kokenyesi *J. Non-Cryst. Solids* **355** 1939 (2009)
- [31] Q Yan, H Jain, J Ren, D Zhao and G Chen *J. Phys. Chem. C* **115** 21390 (2011)
- [32] A Lorinczi *J. Opt. Adv. Mater.* **1** 37 (1999)
- [33] S K Tripathi, S Gupta, F I Mustafa, N Goyal and G Saini *J. Phys. D Appl. Phys.* **42** 185404 (2009)
- [34] X Su, R Wang, B Luther-Davies and L Wang *Appl. Phys. A* **113** 575 (2013)
- [35] A V Kolobov *Photo-Induced Metastability in Amorphous Semiconductors* (Weinheim: Wiley-VCH) (2003)
- [36] M Jin, C Ping, P Boolchand, T Rajagopalan, K L Chopra, K Starbova and N Starbova *Phys. Rev. B* **78** 214201 (2008)
- [37] R Chauhan, A K Srivastava and A Tripathy *Prog. Nat. Sci. Mater. Int.* **20** 54 (2010)
- [38] K Tanaka *Thin Solid Films* **66** 271 (1980)
- [39] S H Wemple *Phys. Rev. B* **7** 3767 (1973)
- [40] N K Sahoo, S Thakur, R B Tokas, A Biswas and N M Kamble *Appl. Surf. Sci.* **253** 3455 (2007)
- [41] A Ganjoo, K Shimakawa, H Kamiya, E A Davis and J Singh *Phys. Rev. B* **62** R14601 (2000)
- [42] A Ganjoo and H Jain *Phys. Rev. B* **74** 024201 (2006)
- [43] J Tauc *The Optical Properties of Solids* (Amsterdam: North-Holland) (1970)
- [44] R A Smith *Philos. Mag. Suppl.* **2** 81 (1953)
- [45] N F Mott and E A Davis *Electronics Processes in Non-Crystalline Materials* (Oxford: Clarendon) p 428 (1979)
- [46] M L Theye *Proceeding of Vth International Conference on Amorphous and Liquid Semiconductors* **1** 479 (1974)
- [47] T T Nang, M Okuda, T Matsushita, S Yokota and A Suzuki *Jpn. J. Appl. Phys.* **14** 849 (1976)
- [48] T T Nang, M Okuda and T Matsushita *Phys. Rev. B* **19** 947 (1979)
- [49] T Kawaguchi and S Maruno *J. Appl. Phys.* **73** 456 (1993)
- [50] W-H Wei, S Xiang, S-W Xu, L Fang and R P Wang *J. Appl. Phys.* **115** 183506 (2014)
- [51] P Knotek, L Tichy, D Arsova, Z G Ivanova and H Ticha *Mater. Chem. Phys.* **119** 315 (2009)
- [52] J Tauc *Amorphous and Liquid Semiconductors* (New York: Plenum Press) p 159 (1979)
- [53] F Urbach *Phys. Rev.* **92** 1324 (1953)
- [54] S R Elliott *The Physics and Chemistry of Solids* (Wiley: Chichester) (1998)
- [55] G D Cody *Phys. Rev. Lett.* **47** 1480 (1981)
- [56] J Heo, J S Sanghera and J D Mackenzie *J. Non-Cryst. Solids* **101** 23 (1988)
- [57] R P Wang, A V Rode, D Y Choi and B Luther-Davies *J. Appl. Phys.* **103** 083537 (2008)
- [58] L Pauling *The Nature of the Chemical Bond* (Ithaca: Cornell University Press) p 664 (1960)
- [59] K Jackson, A Briley, S Grossman, D V Porezag and M R Pederson *Phys. Rev. B* **60** R14985 (1999)
- [60] J H Baeck, T H Kim, H J Choi, K H Jeong and M H Cho *J. Phys. Chem. C* **115** 13462 (2011)
- [61] G Lenz et al. *Opt. Lett.* **25** 254 (2000)
- [62] Z G Ivanova, V Pamukchieva and M Vleck *J. Non-Cryst. Solids* **293–295** 580 (2001)
- [63] P Sharma, V S Rangra, P Sharma and S C Katyal *J. Alloys Compd.* **480** 934 (2009)